Hindawi
Scientific Programming
Volume 2022, Article ID 2227049, 12 pages
https://doi.org/10.1155/2022/2227049

Research Article

Monitoring, Prediction, and Evaluation of Mountain Geological Hazards Based on InSAR Technology

Fan Yang,[1,2] Zhongrong Jiang,[1] Junqian Ren,[2,3] and Jian Lv[1,2,4]

[1]*SiChuan HuaDi Building Engineering Co. Ltd, Chengdu 610081, China*
[2]*Chengdu University of Technology, Chengdu 610059, China*
[3]*Sichuan Highway Planning, Survey, Design and Research Institute Ltd, Chengdu 610041, China*
[4]*School of Geographic Science and Remote Sensing, Guangzhou University, Guangzhou 510006, China*

Correspondence should be addressed to Jian Lv; 1819500009@e.gzhu.edu.cn

Received 23 November 2021; Accepted 18 December 2021; Published 17 January 2022

Academic Editor: Le Sun

When traditional geological hazard survey methods are used for deformation monitoring in mountainous areas, it often shows the disadvantages of low applicability of monitoring methods and limited accuracy of detection results. In recent years, synthetic aperture radar interferometry (InSAR) technology has incomparable advantages in surface deformation monitoring, such as all-weather detection, wide detection range, high detection accuracy, and low detection cost. At the same time, InSAR technology can also provide data and technical support for the subsequent task of potential geological disaster point identification and geological disaster risk zoning in the study area. Alos-2 radar is selected; in this paper the satellite image is the research data, and the InSAR technology is used to complete the surface deformation detection. Then, based on the previous surface deformation monitoring results, the potential geological disaster points in the study area are extracted, and the distribution law and incubation conditions of the disaster points are analyzed and described. According to the field conditions of a certain area, the surface distribution, development causes, and inducing mechanism of the potential geological disaster points are explored; the results show that the development of geological disasters in the study area is affected by many factors such as landform, geological environment, climate, hydrology, and human activities. Based on this, 11 factors such as formation lithology, slope, and river are used as evaluation factors for mountain geological disaster monitoring, prediction, and evaluation analysis. Finally, the improved analytic hierarchy process information model is used to complete the monitoring, prediction, evaluation, and analysis of regional geological hazards in the study area. In this paper, the improved AHP-information method is used to classify the risk of mountain geological disasters in the study area. Finally, the evaluation results are verified, which proves that the improved AHP-information method is reliable, and its mountain geological disaster monitoring and prediction evaluation effect is better than the traditional AHP-information method.

1. Introduction

Under the influence of basic geographical environment factors such as fragile geological environment, huge topographic relief, and complex stratum lithology, the regional surface deformation of mountains in some areas is active [1]. In addition, under the trigger of strong geological tectonic movement, rainfall, and other factors, all kinds of geological disasters in the county show a trend of frequent occurrence, easy occurrence, and high incidence for a long time [2]. Due to the special topographic and geological conditions and abundant vegetation coverage in the study area, geological disasters are concealed, which makes it difficult to realize early prediction in the process of disaster prevention and control and easily causes large-scale social, economic, and personnel losses [3]. When the traditional geological hazard survey method is used to monitor the deformation in mountainous areas, it often shows the shortcomings of low applicability of the monitoring method and limited accuracy of the detection results [4]. Therefore, through the InSAR

technology, to effectively identify the potential geological disasters and to prevent and control become the focus of this paper [5, 6].

2. InSAR Technology

Usually, InSAR technology is applied to DEM construction and surface deformation monitoring [6]. In the early stage of the development of InSAR technology, due to the defects of some characteristics of radar images, the surveying and mapping accuracy is limited. In recent years, with the improvement of interferometry technology and the establishment of many SAR satellite systems, InSAR technology has been more mature applied to topographic survey and deformation monitoring [7].

2.1. InSAR Fundamentals. InSAR technology can be used to complete the task of acquiring DEM data. The key principle of this technology is to realize two or more observation processes in the same research area, and different observation processes are required to have proper viewing angle difference during imaging, so as to achieve the purpose of acquiring single-view complex images with high coherence [8]. Then, the image interference processing flow is completed in turn, and the Earth surface elevation data is extracted according to its interference phase information. Complete the above series of operations, that is, to realize the construction of DEM in the research area [9].

Figure 1 shows the geometric relationship diagram when InSAR system observes the surface and obtains the surface elevation information. In Figure 1, S_1 and S_2 represent the position of radar antenna during two imaging processes, which can be obtained from the orbital parameters of the satellite itself, and B is the spatial distance between them, which is called baseline. R_1 and R_2 are the oblique distances from the two antennas to the ground observation points, respectively. α represents the angle between the baseline and the horizontal direction, θ is the incident angle, H is the height of the antenna track, and h is the elevation of the measured ground point target relative to the reference ellipsoid.

The phase information contained in radar echo signal can be divided into two parts: one is the phase information reflecting the characteristics of the target point itself, and the other is the phase value representing the distance between the ground point and the antenna. This kind of information is the part that can be used to retrieve the position of the ground target point. In the course of two radar observations, the ground target point can be regarded as unchanged, so the characteristic phase of the target point itself is consistent in each radar echo signal. Therefore, from the phase information of the distance between the target and the antenna, we can know that the echo signal of the antenna S_1 is

$$\phi_1 = 2\pi \frac{2\mathrm{R}_1}{\lambda}. \tag{1}$$

The echo signal phase of antenna S_2 is

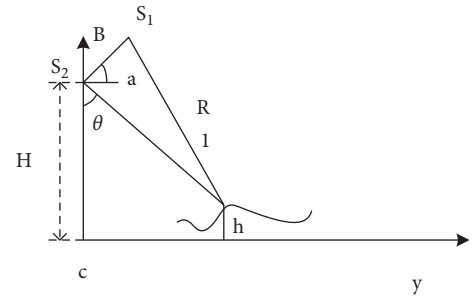

Figure 1: Geometric diagram of InSAR system.

$$\phi_2 = 2\pi \frac{2\mathrm{R}_2}{\lambda}, \tag{2}$$

where λ is the wavelength of radar signal. In this way, the interference phase difference between two images can be expressed:

$$\Delta\phi = \phi_1 - \phi_2 = -\frac{4\pi}{\lambda}\left(\mathrm{R}_1 - \mathrm{R}_2\right) = -\frac{4\pi}{\lambda}\delta. \tag{3}$$

In the process of generating interferogram, due to the difference of incident angle and azimuth, the objects with the same name in two SAR images cannot be completely aligned, so it is necessary to register them. After the registration operation is completed, the interference phase difference in equation (3) can be obtained from the generated interferogram by using the processed image to complete the multiplex multiplication [10]. It can be seen from equation (3) that, for the same ground target point, the echo phase difference is proportional to the oblique distance difference. After two echo signals from the same target unit are multiplied together, the phase difference obtained is only determined by the oblique distance difference, which is related to the elevation of the ground unit. From the geometric relationship information shown in Figure 1, equation (4) can be obtained:

$$\mathrm{R}_2^2 = \mathrm{R}_1^2 + \mathrm{B}^2 - 2\mathrm{R}_1\mathrm{B}\cos\left(\alpha + \frac{\pi}{2} - \theta\right). \tag{4}$$

Make a transformation to get

$$\sin(\theta - \alpha) = \frac{R_1^2 - R_2^2 + B^2}{2R_1B} = \frac{\left(R_1 + R_2\right)}{2R_1B} + \frac{B}{2R_1}. \tag{5}$$

According to the actual situation of SAR system observation, baseline B can be ignored compared with R_1 and R_2 alone, and at the same time, $(R_1 - R_2)$ is far less than R_1. By transforming equation (5), we can get

$$\sin(\theta - \alpha) \approx \frac{R_1 - R_2}{B} = -\frac{\lambda\Delta\varphi}{4\pi B}. \tag{6}$$

Thus, α, B, and H are obtained from the orbital attitude data, and from the geometric relationship shown in Figure 1:

$$h = H - R_1\cos\theta. \tag{7}$$

In the actual operation process, after the data undergoes triangulation operation, the interference solution result

obtained is the main value of its phase information, which is always between $[-\pi, \pi]$, and its true value can be obtained only after subsequent phase unwrapping.

2.2. D-InSAR Technology. The key of D-InSAR technology is to make two or more SAR images in the same area complete the process of differential interference, from which the surface deformation data of the study area can be obtained [11]. The deformation information can be expressed by the observation and imaging results of radar antennas for the same target objects. That is, when there is surface deformation, the phase reflecting the spatial position change between the ground target and the observation antenna can be extracted from the image pair interference processing results, so as to realize the regional deformation monitoring. After two previous observation and imaging processes are completed, the interference phase can be obtained from the interference measurement results at this time. The key components of the interference phase can be divided into: morphological phase (φ_{def}), reference ellipsoid phase (φ_{o}), terrain phase (φ_{topo}), atmospheric phase (φ_{atm}), random noise phase (φ_{noise}), etc., which are expressed by formula (8) as follows:

$$\varphi = \varphi_{\text{def}} + \varphi_o + \varphi_{\text{topo}} + \varphi_{\text{atm}} + \varphi_{\text{noise}}. \tag{8}$$

In the process of regional surface deformation monitoring noise phases such as reference ellipsoid atmosphere and terrain will have great interference on deformation detection. These error phases should be removed as much as possible to obtain more accurate regional surface deformation monitoring results. According to the difference of the methods of obtaining the terrain phase φ_{topo} process, the synthetic aperture radar differential interferometry is divided into two-pass, three-pass, and four-pass methods, which is still the main method to realize D-InSAR.

2.2.1. Fundamentals. In the actual process of D-InSAR, the terrain phase is obtained by converting the digital elevation data from outside to the radar system. The process of removing the terrain phase information from the original interference results is another core content besides the interference to the differential interference when using D-InSAR to detect the regional surface deformation. Figure 2 shows a geometric schematic diagram of obtaining surface deformation by two-orbit D-InSAR [12, 13].

Similar to the principle of InSAR altimetry, point P in the figure is the ground point observed by satellites twice, S_1 and S_2 are antenna positions, f represents the distance difference between the two antennas S_1 and S_2 and the ground observation point P, α is the angle between the baseline and the horizontal direction, and θ is the incident angle. At this time, the observation point P itself has a displacement of Δd in the line of sight. The surface deformation information of the study area can be solved by calculating the phase change phase, and the calculation formula is as

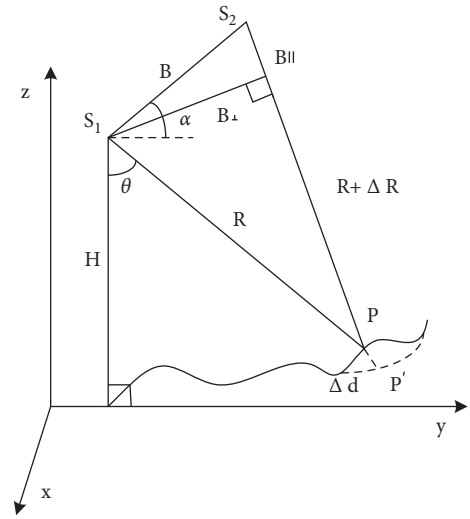

Figure 2: Geometric schematic diagram of two-orbit D-InSAR.

$$\varphi_{\text{def}} = \varphi - \varphi_o - \varphi_{\text{topo}}. \tag{9}$$

$$\Delta \text{d} = \frac{4\pi}{\lambda}\varphi_{\text{def}}, \tag{10}$$

where λ is the wavelength of the band; Δd is the deformation along the radar line of sight. It can be seen from the formula that, assuming that the phase value obtained from the differential interferometry results has a periodic change of 2π, the specific value of the relative regional surface deformation Δd is half wavelength length $\lambda/2$, which indicates that D-InSAR is highly sensitive to surface deformation. The expression process of equation (9) belongs to the case where the error phases such as atmosphere and reference ellipsoid are ignored for convenience of understanding. D-InSAR technology can monitor centimeter-level or even sub-centimeter-level microdeformation, which greatly improves the monitoring ability of surface deformation monitoring means.

2.2.2. Data Processing Flow. When D-InSAR is used to obtain surface deformation information by differential processing of interference phase, its data processing flow is shown in Figure 3.

The core of D-InSAR technique for ground deformation calculation is the differential processing of interference phase. The data processing flow is roughly divided into three parts: data preprocessing, differential interference calculation, and deformation calculation.

2.3. SBAS-InSAR Technology. Short baseline subset method is proposed by Berardino et al. on the basis of previous research results. When using this technology to generate interferogram, it requires short spatiotemporal baseline interference pairs, which can effectively reduce temporal decoherence and spatial decoherence [14].

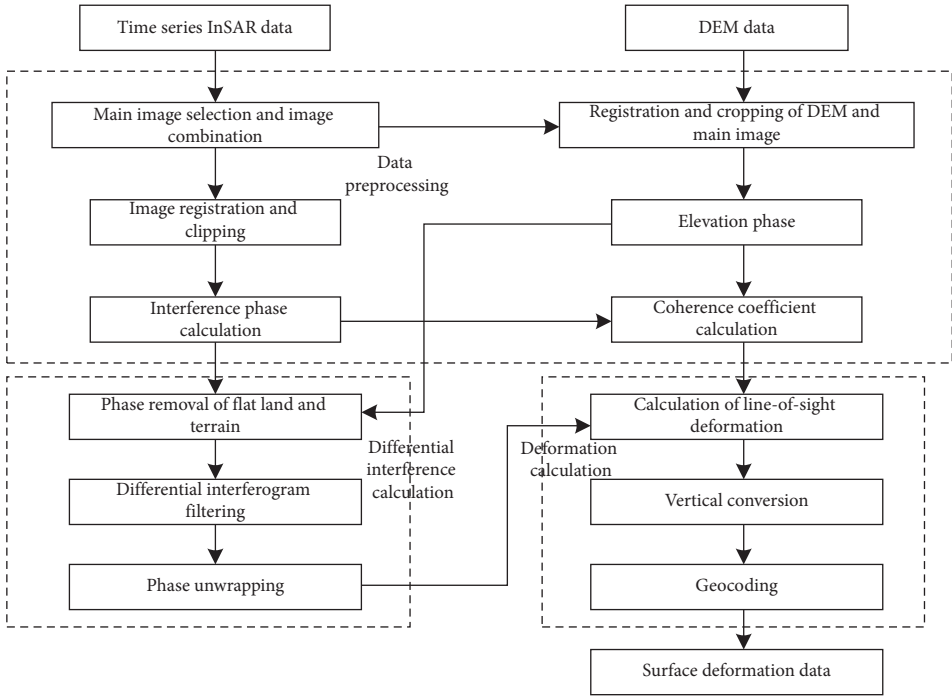

Figure 3: Flowchart of D-InSAR processing.

2.3.1. Fundamentals. An important step in the realization of SBAS-InSAR technology is to complete the subset division of all SAR images. This process is to divide the image set into different short baseline subsets according to the influence of spatial and temporal baselines on the coherence of images and complete the calculation of interference phase of each image pair in the subset. At this time, the number of interference pairs is obviously increased, and the coherence of each interferogram is also enhanced compared with the previous case where only a single main image is used. The differential interferograms are linked by singular value decomposition (SVD), which can restrain the effect of DEM error and atmospheric phase delay on the phase variation and finally obtain the least square solution.

The specific process is as follows:

(1) Assuming there are N+1 SAR images in $[t_o, t_1, t_2, t_3, \ldots, t_n]$ time period, the interference pairs with M pairs of spatiotemporal baselines within the threshold condition can be obtained by any combination, and M should meet the requirements of equation.

$$\frac{N}{2} \leq M \leq \frac{N(N-1)}{2}. \tag{11}$$

Assuming that the i-th interferogram is obtained by removing terrain phase, filtering interferogram, and unwrapping phase, the time of acquisition of main image and slave image is t_B and t_A, respectively, and the interference phase at (a, r) in radar coordinate system can be expressed as

$$\Delta\varphi_i(a,r) \approx \frac{4\pi}{\lambda}\left[d_{t_A}(a,r) - d_{t_B}(a,r)\right]. \tag{12}$$

$d_{t_A}(a,r)$ and $d_{t_B}(a,r)$ are the phases of the pixels (a, r) at time t_A and time t_B relative to the initial time t_0, respectively, and λ is the wavelength of the band.

(2) At time = t_0, $d_0 = 0$, the vector corresponding to the phase of the sequential SAR image is expressed as

$$\varphi^t = [\varphi_1, \cdots, \varphi_n]. \tag{13}$$

At the pixel (a, r), let IE be the master image and IS be the slave image, corresponding to all M interference pairs:

$$\begin{cases} \mathrm{IE} = [\mathrm{IE}_1, \cdots, \mathrm{IE}_M] \\ \mathrm{IS} = [\mathrm{IS}_1, \cdots, \mathrm{IS}_M] \end{cases}. \tag{14}$$

Then the phase of all differential interferograms is

$$\Delta\varphi_i(a,r) = \varphi\left(t_{IE_i}\right) - \varphi\left(t_{IS_i}\right), \tag{15}$$

where $t_{IE_i} > t_{IS_i}$, $i = 1, 2, \ldots, M$, can be expressed as

$$\Delta\varphi = G\varphi. \tag{16}$$

In formulas (3)–(16), G is a matrix of order $M \times N$, which represents a system of equations composed of N unknowns and M equations. It can be seen that, in the matrix, each row

corresponds to a differential interference pair, and each column represents the corresponding SAR images from t_0 to t_N in turn.

When the interference pairs are located in the same small baseline set, the least square method is used to estimate the deformation value of the time series in the subset. When there are multiple subsets and the matrix is not rank matrix, the SVD method should be used to realize the joint solution of the subsets, so as to extract the cumulative deformation results on the time series.

2.3.2. Data Processing Flow. In the processing flow of SBAS-InSAR technology, the key to the realization of this technology is to construct a number of interference pair subsets reasonably. This process requires that the combined spatiotemporal baseline of each subset of internal interference pairs should be in the threshold range needed to form a high-quality interferogram. This technique can be simply understood as the interferometric measurement method of the surface deformation change process in the study area during the study period by solving the differential interference phase in the time series.

The flow of surface deformation detection using SBAS-InSAR method is shown in Figure 4. Its data processing flow includes data preprocessing, differential interference calculation, time and space deformation estimation, and so on.

3. Monitoring, Prediction, and Evaluation of Mountain Geological Disasters Based on Improved AHP-Information Quantity Method

In recent years, the frequent geological disasters in China not only cause serious economic losses to the society, but also seriously threaten people's lives and disturb the normal life of residents, which has aroused widespread concern from people from all walks of life [15]. Therefore, the identification of potential geological hazards and the study of their spatial and temporal distribution are of great significance in disaster prevention and control, and at the same time, it is also the premise of further quantitative analysis of geological hazards.

The information of mountain surface deformation detected by InSAR technology has high reliability and accuracy, which is the basis of early identification of potential geological disasters. Combined with GIS spatial analysis and visual interpretation, the hidden danger points of potential geological disasters can be extracted, and the deformation characteristics of mountain surface in time and space can be further analyzed [16].

At present, there are many statistical analysis models for geological disaster risk analysis. When the information quantity method of information theory is applied to the risk assessment of geological disasters, it has the characteristics of combining qualitative and quantitative analysis. According to the influence degree of different influencing factors on geological disasters, the risk of geological disasters can be effectively assessed. Analytic Hierarchy Process (AHP) is a fast method to determine weights, which can be used to assign weights to different evaluation factors in geological hazard risk assessment [17, 18]. In this paper, the weighted information model based on AHP is adopted, which not only considers the advantages of AHP that fully considers the subjective experience of experts, but also combines with the objective information in the information model [19, 20].

3.1. Information Quantity Method. The information quantity method originated in the United States, and in China, it was first quoted by Professor Yan Tongzhen to predict the surface landslide and then gradually widely used in the geological disaster risk assessment in the geological disaster-prone areas in China. As far as the information quantity method itself is concerned, its central idea is to use the information quantity value to reflect the difficulty of geological disasters in the study area based on the information quantity contributed by various influencing factors to geological disasters [21]. This method is practical and simple and can be used to predict the development law of geological disasters. In general, the information quantity value is used as a quantitative index to quantitatively describe the risk of geological disasters with probability situation. The greater the information quantity value obtained, the more likely the geological disasters to occur, and vice versa.

3.1.1. Basic Theoretical Model. When applying the method of information quantity to realize the risk assessment of geological hazards, the information quantity provided by the actual geological disasters is used to express the action degree of each influencing factor with information quantity, which can reflect the contribution degree of these influencing factors to the development of surface geological disasters. For geological disaster event B, X_{ij} is the factor affecting its occurrence (where $i = 1, 2, \ldots, n$, I is the selected disaster influencing factor; $J = 1, 2, \ldots, M$, and J is the subinterval divided by each influencing factor); then the $I_{X_{ij} \longrightarrow B}$ expression of geological disaster information provided by a single influencing factor is as follows:

$$I_{X_{ij} \longrightarrow B} = \ln \frac{P\left(B/X_{ij}\right)}{P(B)} \ (j = 1, 2, \cdots, n). \tag{17}$$

Among them, $P(B/X_{ij})$ corresponds to the development probability of geological disaster class B in the J section within the disaster impact factor X_i; $P(B)$ represents the regional background value, that is, the probability of occurrence of ground disaster B under the regional background conditions; N represents the number of selected types of disaster impact factors; M represents the number of secondary impact factor segments divided by each disaster impact factor.

In the process of actual data processing, it is often impossible to directly obtain the data needed to calculate the information amount of geological disasters. Under normal circumstances, in order to facilitate subsequent calculation, the probability value represented by $P(B/X_{ij})$ is selected to be

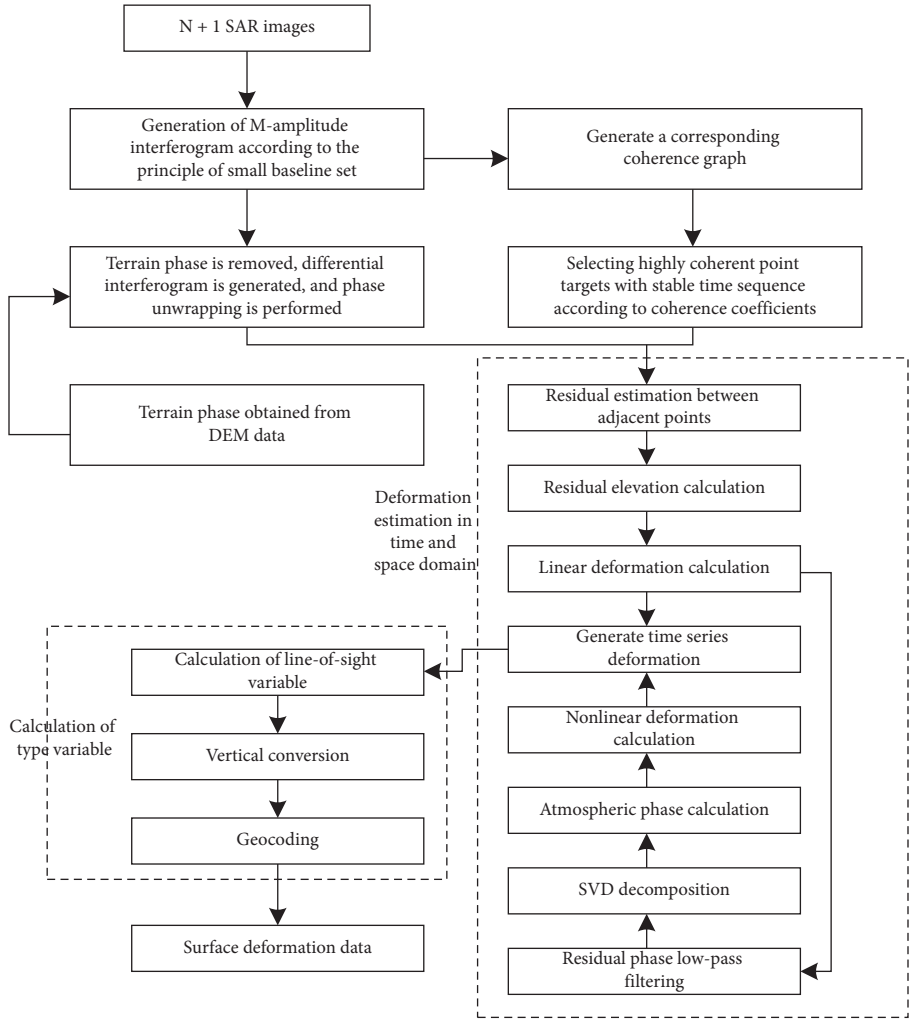

Figure 4: SBAS-InSAR data processing flow.

converted into the sample frequency value. The specific calculation formula is as follows:

$$I_{X_{ij} \longrightarrow B} = \ln \frac{N_{ij}/S_{ij}}{N/S} \ (j = 1, 2, \cdots, n). \tag{18}$$

Among them, the value $I_{X_{ij} \longrightarrow B}$ can represent the amount of information provided by the J section for the development of geological disaster class B within the disaster impact factor X_i; N_{ij} represents the area value or the number of development points of disaster B in the J section within the disaster impact factor X_i; N_{ij} represents the distribution area value of the J section in the study area in the disaster impact factor X_i; N represents the area value covered by all geological disasters or the number of all developed geological disasters in the whole study area; S represents the total area of the whole study area.

The actual process of geological hazard risk assessment in the study area is to divide the study area into several assessment units and finally need to calculate and obtain the comprehensive information value of each assessment unit. To sum up, the information value is affected by the combination of various influencing factors, and the comprehensive information value I of all evaluation units can be calculated by using the following formula:

$$I = \sum_{i=1}^{n} I_{X_{ij} \longrightarrow B}. \tag{19}$$

Using information quantity model to complete the study of regional disaster risk assessment in a specific study area can be understood as taking each evaluation unit as an independent research unit and taking each evaluation factor as the premise of risk assessment, calculating the total information quantity of each independent research unit, and comparing the calculated information quantity values. The specific information value obtained from the above operations can be used to indicate that when the independent evaluation unit to which the information belongs is affected by various geological disaster influencing factors, the probability of geological disasters is greater, indicating that

the geographical area where the evaluation unit is located is more likely to break out geological disasters, and it is necessary to focus on monitoring and take timely prevention and control measures.

3.1.2. Weighted Information Volume Model. In order to enhance the accuracy of the evaluation results, this study takes the conventional information as the premise, supplemented by the corresponding weight value of each evaluation factor to complete the whole evaluation process. Generally speaking, the conventional process of information calculation is based on the effect degree of various influencing factors on the development of geological disasters in the evaluation unit layer. Conventional information quantity model can be understood as the idea that, in the process of calculating information quantity, the weight of all factors is given to 1, while weighted information quantity method can apply subjective experience of experts to the evaluation process according to objective facts, which has higher rationality and reliability.

The weight W_i of evaluation factors at all levels is obtained by the weight acquisition method, and the total value of weighted information I_w is

$$I_{\mathrm{w}} = \sum_{i=1}^{n} W_i I_{X_{ij} \longrightarrow B}, \tag{20}$$

where $I_{X_{ij} \longrightarrow B}$ is the information value of a single influencing factor.

When the weighted information model is used to evaluate the hazard of land disasters in the study area, the evaluation index is the total information value $I_{w.}$. When evaluating the risk of geological disasters in each geographical unit, the probability of occurrence increases with the increase of total information I_w.

Through the previous research on the methods of determining the weight I_w, we can see that the current mainstream methods include analytic hierarchy process, principal component analysis, and so on. In this study, the analytic hierarchy process (AHP) is used to obtain the weight of impact factors, and different weights are given according to the difference of the impact degree of each disaster factor, and the total information weight is obtained by weighting. Weighted information method will complement the advantages of analytic hierarchy process and information method and make the evaluation results more accurate.

3.2. Selection of Evaluation Factors in the Study Area. Through the analysis of the factors affecting the distribution of potential geological disasters and the research results of scholars at home and abroad, it can be seen that the development of geological disasters is affected by many factors. The selection of influencing factors needed in the study should fully consider the availability of data, the scope and environment of the study area, and the requirements of research accuracy. Therefore, in the process of geological hazard risk assessment in different study areas, the selected evaluation factors are usually different.

Combined with the actual geographical conditions of a certain area selected in this paper, the influencing factors of this study area are divided into natural environment factors, social environment factors, and disaster-inducing factors. Among them, the basic natural environment factors are divided into topographic factors (including slope, elevation, aspect, and topographic relief), geological factors (geological structure, stratum lithology), basic features (rivers), ecological factors referring to vegetation coverage, social and environmental factors referring to roads, and inducing factors including earthquakes and rainfall.

In this study, ASTER GDEM elevation data with resolution of 30 m is selected as reference DEM, and on the basis of this data, the slope, aspect, and fluctuation data of the study area are obtained.

Some impact factor data cannot be obtained directly and need to be obtained after certain data processing operations. The specific process of obtaining rainfall in the study area is as follows: the annual average rainfall data of the national meteorological stations in the area and its surrounding counties in recent 15 years are obtained by Kriging spatial interpolation method. In order to facilitate the calculation of the follow-up evaluation process, the operation of properly merging and adjusting rainfall level areas is made. Earthquake intensity data are obtained according to China Seismological Network.

The average annual rainfall in the study area is subdivided into 11 rainfall levels, and the lowest and highest rainfall levels are less than 550 mm and more than 640 mm, respectively. Earthquake intensity is divided into four grades, and the intensity grade decreases around the focal point.

Based on the detailed analysis of the basic data of the experimental area, the pixel dichotomy model is adopted as the acquisition method of vegetation coverage data in this study. That is, the Landsat 8 digital products are processed by using the pixel dichotomy model based on the normalized vegetation index (NDVI), and the formula is as follows:

$$\begin{aligned} \mathrm{NDVI} &= fc \times \mathrm{NDVI}_{\mathrm{veg}} + (1 - fc)\mathrm{NDVI}_{\mathrm{soil}}, \\ fc &= \frac{\left(\mathrm{NDVI} - \mathrm{NDVI}_{\mathrm{soil}}\right)}{\left(\mathrm{NDVI}_{\mathrm{veg}} - \mathrm{NDVI}_{\mathrm{soil}}\right)}, \end{aligned} \tag{21}$$

where fc is vegetation coverage; $\mathrm{NDVI}_{\mathrm{soil}}$ is the normalized vegetation index value of bare soil without vegetation coverage area; $\mathrm{NDVI}_{\mathrm{veg}}$ is the normalized vegetation index value of the area completely covered by vegetation.

In the course of actual hazard assessment, the criteria of assessment factors are as follows: elevation is divided into six grades: <1500 m, 1500 m~2000 m, 2000 m~2500 m, 2500 m~3000 m, 3000 m~3500 m, and > 3500 m; the slope is divided into six grades: 0~10, 10~20, 20~30, 30~40, 40~50, and >50. The slope direction is divided into four directions: north and northeast, east and southeast, south and southwest, west and northwest. The buffer distance of fault zone is defined as 3 km, 6 km and 9 km, and the study is divided into

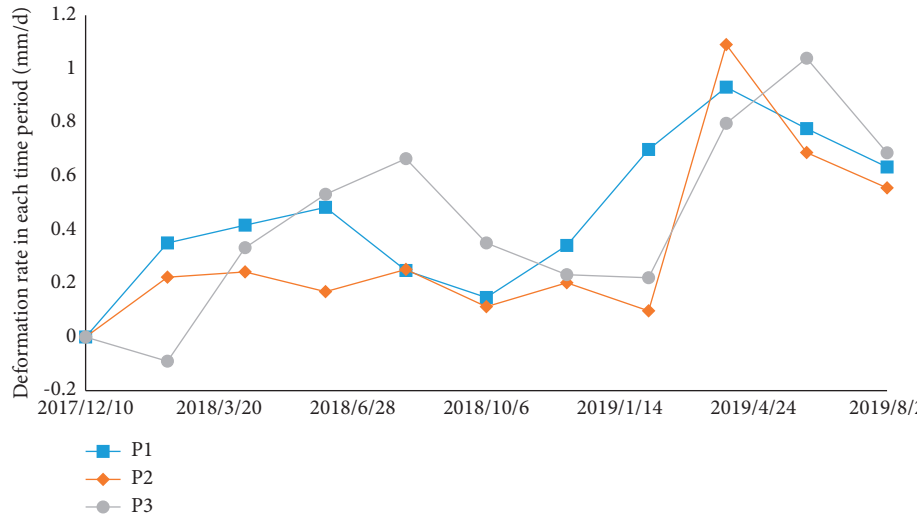

Figure 5: Deformation rate in each period.

five grades of fault zone influence areas. According to the earthquake intensity, the research is divided into four grades: V, VII, Vl, and IX. According to stratigraphic lithology, the study is divided into three areas. According to the average annual rainfall, the study area is divided into five grades: <560 mm, 560 mm~590 mm, 590 mm~620 mm, 620 mm–650 mm, and >650 mm. According to the buffer distance of 0.5 km, 1 km, and 1.5 km, the study area is divided into four grades. The study area is divided into six grades according to the buffer distance of 200 m, 600 m, 1000 m, 1400 m, and 1800m. The topographic relief degree is divided into six grades: ≤100 m, 100 m~200 m, 200 m–300 m, 300 m–400 m, 400 m~500 m, and >500 m. Vegetation coverage is divided into five grades according to <50%, 50%–60%, 60%–70%, 70%–80%, and >80%.

3.3. Determination of Weight of Evaluation Factor. In general, the weight calculation methods include geometric average method, arithmetic average method, and eigenvector method. In order to improve the reliability of the results, this paper abandons the single calculation method used in the conventional thinking and chooses three weight calculation methods instead and takes the average value of each method as the final weight.

The formula of geometric average method is

$$W_i = \frac{\left(\prod_{j=1}^{n} a_{ij}\right)^{1/n}}{\sum_{i=1}^{n}\left(\prod_{j=1}^{n} a_{ij}\right)^{1/n}}, i = 1, 2, \ldots, n. \tag{22}$$

The arithmetic average formula is

$$W_i = \frac{1}{n}\sum_{j=1}^{n}\frac{a_{ij}}{\sum_{k=1}^{n} a_{kj}}, j = 1, 2, \ldots, n. \tag{23}$$

The eigenvector method formula is

$$UW = \lambda_{\max} W, \tag{24}$$

where a_{ij} is the element of the judgment matrix, n is the number of columns of the judgment matrix, and u is the judgment matrix. Average the three calculation results, and get the final weight value of each evaluation factor.

4. Experiment

4.1. Evaluation Process

4.1.1. Analysis of Spatial and Temporal Pattern Distribution Characteristics of Potential Mountain Geological Disaster Points. The deformation information of the three feature points in the time series is counted, and the deformation rate in each period is as shown in Figure 5, and the accumulated deformation is as shown in Figure 6.

4.1.2. Information Quantity Method. In this study, the potential geological hazard points extracted by SBAS-InSAR technology are used as the basic research data for monitoring, forecasting, evaluation, and analysis of mountain geological hazards, and then the information amount is calculated. In this process, the grid unit of 30 m × 30 m is used as the evaluation unit. The information value reflected by the types of secondary influencing factors divided from each evaluation index can be obtained. In practical application, the amount of information is the reference index of the effect degree of each secondary influencing factor on the development of geological disasters in the study area.

See Table 1 for the distribution of each evaluation index and its specific information value in the study area.

According to the meaning of information model, the greater the information value, the easier it is to have geological disasters. When the information value of the secondary influencing factors in the table is greater than 0, it shows that the probability of developing geological disasters under the influence of this factor is above the overall development level of mountain disasters affected by this factor in the study area. By the same token, when the information

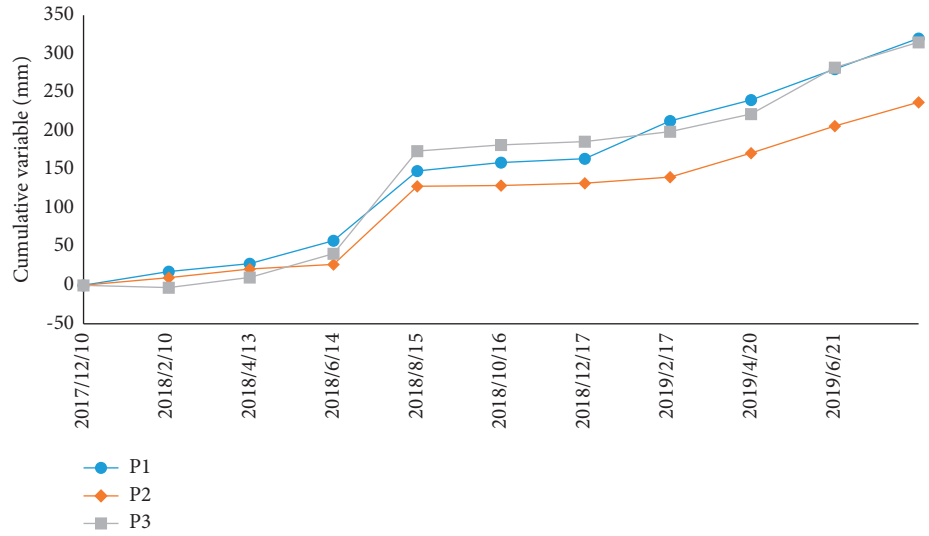

Figure 6: Cumulative deformation.

Table 1: Evaluation factor information scale.

Primary impact factor	Secondary impact factor	Information quantity value (I)	Primary impact factor	Secondary impact factor	Information quantity value (I)
Elevation (unit: m)	<1500	1.527912	Earthquake intensity	VI	−1.018517
	1500–2000	1.878802		VII	−0.305413
	2000–2500	1.217833		VIII	0.371931
	2500–3000	0.069574		IX	2.395062
	3000–3500	−1.16868	Average annual rainfall (unit: mm)	<560	−0.647191
	>3500	−3.18195		560–590	−0.162065
Slope (unit: °)	0–10	−0.19465		590–620	0.1848005
	10–20	−0.60147		620–650	−0.363789
	20–30	0.160048		>650	−0.604173
	30–40	0.060803	Rivers (distance from rivers in km)	<0.5	1.1197684
	40–50	−0.13246		0.5–1	−0.020673
	>50	−0.76925		1–1.5	−1.642546
Aspect of slope	North, northeast	−0.57554		>1.5	−1.944394
	East, southeast	0.34215	Road (distance from road, unit: m)	<200	1.9516436
	South, southwest	0.292185		200–600	1.2565791
	West, northwest	−0.37974		600–1000	0.8739286
Geological structure (distance from fault, unit: km)	<3	0.577263		1000–1400	−0.224026
	3–6	0.176452		1400–1800	−0.668493
	6–9	0.025197		>1800	−1.106742
	>9	−0.68012	Topographic relief (unit: m)	0–100	0.553517
Vegetation coverage	<50%	−0.1233		100–200	0.230892
	50%–60%	0.006014		200–300	−0.339274
	60%–70%	0.392581		300–400	−0.134666
	70%–80%	0.964443		400–500	0.33332
	>80%	0.420331		>500	−2.133569
Stratigraphic lithology	T	−0.04822			
	DCWZE	0.268584			
	CPQ	0.004012			

amount of the secondary influencing factors in the table is less than 0, it means that, in the area where the secondary influencing factors are distributed, the ease of developing geological disasters under the influence of this factor is below the overall development level of mountain disasters affected by this factor in the study area.

4.1.3. Improved Analytic Hierarchy Process. Using the analytic hierarchy process to calculate the weights of evaluation factors, the hierarchical structure model is constructed, as shown in Figure 7. Eleven evaluation factors, including stratum lithology (C1), slope (C2), river (C3), topographic relief (C4), vegetation coverage (C5), average annual rainfall

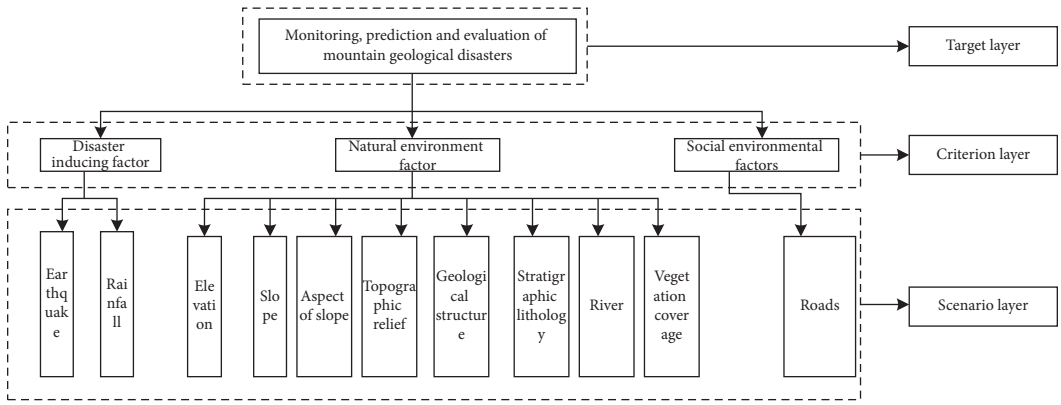

Figure 7: Hierarchical model.

Table 2: Judgment matrix.

	C1	C2	C3	C4	C5	C6	C7	C8	C9	C10	C11
C1	1	2	3	3	4	5	6	7	8	9	9
C2	1/2	1	2	3	4	4	5	7	7	8	9
C3	1/3	1/2	1	2	3	4	5	6	7	7	8
C4	1/3	1/3	1/2	1	2	3	4	5	6	7	7
C5	1/4	1/4	1/3	1/2	1	2	3	5	5	6	6
C6	1/5	1/4	1/4	1/3	1/2	1	2	4	5	6	6
C7	1/6	1/5	1/5	1/4	1/3	1/2	1	3	3	5	5
C8	1/7	1/7	1/6	1/5	1/5	1/4	1/3	1	2	4	3
C9	1/8	1/7	1/7	1/6	1/5	1/5	1/3	1/2	1	2	3
C10	1/9	1/8	1/7	1/7	1/6	1/6	1/5	1/3	1/2	1	2
c11	1/9	1/9	1/8	1/7	1/6	1/6	1/5	1/3	1/3	1/2	1

(C6), geological structure (C7), elevation (C8), earthquake intensity (C9), road (C10), and slope aspect (C11), are selected, and the ranking of factors represents the importance to the formation of geological disasters. The judgment matrix constructed by using the above evaluation factors is shown in Table 2.

The weights of each evaluation factor calculated by geometric average method, arithmetic average method, and eigenvector method are represented by $W1$, $W2$, and $W3$, respectively, and the average value W is calculated as the final weight, as shown in Table 3.

4.2. Verification of Evaluation Results. By getting the information quantity of each evaluation factor, the weight of each evaluation factor is obtained, and the total information quantity of each evaluation unit is obtained when the improved AHP-information quantity method is adopted.

According to the calculation results, the lowest total information value of risk assessment in this area is -1.03541, and the highest is 0.6739. According to the total information value of each evaluation unit obtained in the study area, the natural breakpoint method is used to classify it. The region is divided into four regions, and the information value ranges are low-risk area [−1.03541, −0.5475], medium-risk area (−0.5475, −0.2482], high-risk area (0.2482, 0.0874), and extremely high-risk area (0.0874, 0.6739).

ROC (Receiver Operating Characteristic) curve is a common method widely used to test the accuracy of geological hazard zoning assessment in recent years. In the ROC curve, the vertical axis represents the true positive rate, and in the geological hazard risk assessment, the cumulative percentage of the area from high to low in the study area is used as the ordinate. The horizontal axis represents the false positive rate, i.e., 1−specificity, and the cumulative percentage of the number of real historical geological disasters corresponding to each risk level in the study area is used as the abscissa in the geological disaster risk assessment. By calculating the AUC (Area under Curve) under the ROC curve, the evaluation accuracy of the geological hazard evaluation model is measured.

The value range of AUC is [0, 1], and the higher the value, the better the prediction effect of the model. Usually, we use AUC range (0.5, 0.7], (0.7, 0.8), (0.8, 0.9), (0.9, 1) to indicate low, fair, good, and excellent prediction accuracy, respectively. Figure 8 shows a ROC graph, in which gray lines represent the dividing line with AUC value of 0.5. The AUC values of the improved AHP-information method before and after calculation are 0.812 and 0.854, respectively, and their values are between (0.8, 0.9), indicating that the two models have good effects on the risk assessment and classification of geological disasters. The improved AHP-information model improves the prediction credibility, and the evaluation results can reflect the difficulty of mountain geological disasters in the study area.

Table 3: Weight calculation.

Evaluation factor	W_1	W_2	W_3	W
Stratigraphic lithology	0.2531	0.2512	0.2555	0.2532
Slope	0.2024	0.1962	0.2021	0.2003
River	0.1556	0.1512	0.1553	0.1545
Topographic relief	0.1165	0.1144	0.1145	0.1158
Vegetation coverage	0.0846	0.0855	0.0832	0.0849
Average annual rainfall	0.0643	0.06853	0.0643	0.065
Geological structure	0.0452	0.0492	0.0458	0.0463
Elevation	0.023	0.0291	0.026	0.0277
Earthquake intensity	0.0213	0.0231	0.0210	0.0224
Roads	0.0158	0.0176	0.0158	0.0163

According to the average random consistency index table, RI is 1.52, CI is 0.0842, and CR is $0.05539 < 0.1$, passing the consistency test.

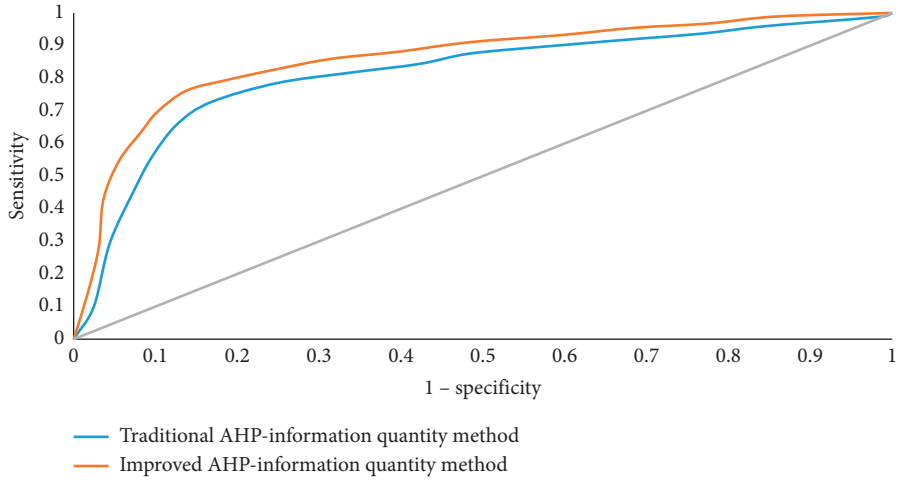

Figure 8: ROC curve.

5. Conclusion

In this paper, the evaluation factors are obtained according to the existing research results and the actual situation. Then, the traditional analytic hierarchy process using a single method to calculate the weights is improved, the geometric average method, arithmetic average method, and eigenvector method are selected to obtain the weights, and the average value is determined as the final weight. In this paper, the improved AHP-information method is used to classify the risk of mountain geological disasters in the study area. Finally, the evaluation results are verified, which proves that the improved AHP-information method is reliable, and its mountain geological disaster monitoring and prediction evaluation effect is better than the traditional AHP-information method. There is no in-depth research on target recognition accuracy, so it is necessary to combine multisensor data with SAR data such as images for comprehensive analysis, which can improve the monitoring effect and application value of mountain geological disasters.

Data Availability

The experimental data used to support the findings of this study are available from the corresponding author upon request.

Conflicts of Interest

The authors declare that they have no conflicts of interest regarding this work.

References

[1] M. Rao and S. A. Gillani, "Active surface deformation from DEM based surface dynamics in upstream of mangla reservoir and eastern potwar plateau," *International Journal of Innovations in Science & Technology*, vol. 2, no. 2, pp. 51–60, 2020.

[2] J. W. Goodge, "Geological and tectonic evolution of the Transantarctic Mountains, from ancient craton to recent enigma," *Gondwana Research*, vol. 80, pp. 50–122, 2020.

[3] C. Xiong, F. Ji, C. Zhou, and Y. Pan, "Investigation and motion characteristics analysis of dangerous rock in high and steep slope based on UAV," *IOP Conference Series: Earth and Environmental Science*, vol. 569, Article ID 012002, 2020.

[4] M. Yu and J. Chao, "Remote sensing investigation of geological hazards in xingguo county, jiangxi province," *E3S Web of Conferences*, vol. 131, no. 5, Article ID 01056, 2019.

[5] Z. Hu, B. Li, Y. Liu, and X. Niu, "Research on quality improvement method of deformation monitoring data based on InSAR," *Journal of Visual Communication and Image Representation*, vol. 64, Article ID 102652, 2019.

[6] Y. Yang, Y. Sun, S. Wu et al., "Surface deformation monitoring of a section of gongyu expressway based on SBAS-InSAR technology," *E3S Web of Conferences*, vol. 233, no. 4, Article ID 01149, 2021.

[7] A. M. Ruiz-Armenteros, M. Marchamalo-Sacrsitán, M. Bakoň et al., "Monitoring of an embankment dam in southern Spain based on Sentinel-1 Time-series InSAR," *Procedia Computer Science*, vol. 181, no. 3, pp. 353–359, 2021.

[8] L. Teixeira, M. R. Oswald, M. Pollefeys, and M. Chli, "Aerial single-view depth completion with image-guided uncertainty estimation," *IEEE Robotics and Automation Letters*, vol. 5, no. 2, pp. 1055–1062, 2020.

[9] Y.-s. Tang, Z.-z. Yin, L.-g. Zhang, Q.-j. Guo, J.-z. Cao, and J.-j. Tong, "The application of the DEM-based burnup construction method in the pebble burnup history analysis in HTR-10," *Nuclear Engineering and Design*, vol. 349, no. AUG, pp. 1–7, 2019.

[10] R. Zhang, C. Meng, C. Wang, and Q. Wang, "Compressed sensing reconstruction of radar echo signal based on fractional fourier transform and improved fast iterative shrinkage-thresholding algorithm," *Wireless Communications and Mobile Computing*, vol. 2021, no. 2, pp. 1–15, 2021.

[11] R. Zhang, Z. Tang, D. Luo, H. Luo, S. You, and T. Zhang, "Combined multi-time series SAR imagery and InSAR technology for rice identification in cloudy regions," *Applied Sciences*, vol. 11, no. 15, p. 6923, 2021.

[12] D. Bekaert, A. L. Handwerger, P. Agram, and D. B. Kirschbaum, "InSAR-based detection method for mapping and monitoring slow-moving landslides in remote regions with steep and mountainous terrain: an application to Nepal," *Remote Sensing of Environment*, vol. 249, no. 1, Article ID 111983, 2020.

[13] J. Widodo, Y. Izumi, A. Takahashi, H. Kausarian, D. Perissin, and J. T. Sri Sumantyo, "Detection of peat fire risk area based on impedance model and DInSAR approaches using ALOS-2 PALSAR-2 data," *IEEE Access*, vol. 7, pp. 22395–22407, 2019.

[14] G. Wang, Y. Wang, X. Zang, J. Zhu, and W. Wu, "Locating and monitoring of landslides based on small baseline subset interferometric synthetic aperture radar," *Journal of Applied Remote Sensing*, vol. 13, no. 4, p. 1, 2019.

[15] K. Konagai, "More than just technology for landslide disaster mitigation: signatories to the Kyoto Landslide Commitment 2020—No. 3," *Landslides*, vol. 18, no. 1, pp. 1951–1957, 2021.

[16] I. Abdulrahman and G. Radman, "Power system spatial analysis and visualization using geographic information system (GIS)," *Spatial Information Research*, vol. 28, no. 4, pp. 101–112, 2019.

[17] U. Goel, K. P. Gupta, and R. Manrai, "Analyzing the factors that affect the adoption of payments banks services in India: an Analytic Hierarchy Process (AHP) approach," *International Journal of Business Information Systems*, vol. 1, no. 1, p. 1, 2020.

[18] F. Imron and M. Rum, "Modernization readiness analysis of Belitang irrigation system at region level using analytic hierarchy process (AHP) method," *IOP Conference Series: Earth and Environmental Science*, vol. 644, no. 1, Article ID 012070, 2021.

[19] X. Ning, K. Gong, W. Li, L. Zhang, X. Bai, and S. Tian, "Feature refinement and filter network for person re-identification," *IEEE Transactions on Circuits and Systems for Video Technology*, vol. 31, no. 9, pp. 3391–3402, 2021.

[20] S. Qi, X. Ning, G. Yang et al., "Review of multi-view 3D object recognition methods based on deep learning," *Displays*, vol. 69, no. 1, Article ID 102053, 2021.

[21] Y. Jiang, J. Zou, X. Hu et al., "Study on optimal laminographic tilt angle: a method for analyzing quantity information gained in projections," *IEEE Access*, vol. 8, pp. 38164–38173, 2020.